THE AMERICAN SOCIETY OF MECHANICAL ENGINEERS
345 E. 47th St., New York, N.Y. 10017

97-GT-270

A DETAILED ANALYSIS OF FILM COOLING PHYSICS PART II. COMPOUND–ANGLE INJECTION WITH CYLINDRICAL HOLES

Kevin T. McGovern and James H. Leylek
Department of Mechanical Engineering
Clemson University
Clemson, SC 29634

ABSTRACT

Detailed analyses of computational simulations with comparisons to experimental data were performed to identify and explain the dominant flow mechanisms responsible for film cooling performance with compound angle injection, Φ, of 45°, 60°, and 90°. A novel vorticity and momentum based approach was implemented to document how the symmetric, counter–rotating vortex structure typically found in the crossflow region in streamwise injection cases, becomes asymmetric with increasing Φ. This asymmetry eventually leads to a large, single vortex system at Φ=90° and fundamentally alters the interaction of the coolant jet and hot crossflow. The vortex structure dominates the film cooling performance in compound angle injection cases by enhancing the mixing of the coolant and crossflow in the near wall region, and also by enhancing the lateral spreading of the coolant. The simulations consist of fully–elliptic and fully–coupled solutions for field results in the supply plenum, film–hole, and crossflow regions and includes surface results for adiabatic effectiveness η and heat transfer coefficient h. Realistic geometries with length–to–diameter ratio of 4.0 and pitch–to–diameter ratio of 3.0 allowed for accurate capturing of the strong three–way coupling of flow in this multi–region flowfield. The cooling configurations implemented in this study exactly matched experimental work used for validation purposes and were represented by high quality computational grid meshes using a multi–block, unstructured grid topology. Blowing ratios of 1.25 and 1.88, and density ratio of 1.6 were used to simulate realistic operating conditions and to match the experiments used for validation. Predicted results for η and h show good agreement with experimental data.

NOMENCLATURE

Cp	pressure coefficient=$p/(1/2\rho V^2)_\infty$
D	film–hole diameter
DR	density ratio = ρ_j/ρ_∞
h	heat transfer coefficient in the presence of film cooling jets = $q''/(T_{aw}-T_w)$, (W/m^2K)
h_o	heat transfer coefficient in the absence of film cooling jets (reference) = $q_o''/(T_\infty-T_w)$, (W/m^2K)
LE	leading edge of streamwise injection film–hole at exit plane
L	length of film–hole
L/D	length–to–diameter ratio of film–hole
M	blowing (or mass flux) ratio = $(\rho V)_j/(\rho V)_\infty$
q″	surface heat flux per unit area (W/m^2)
p	static pressure (Pa)
P	pitch (or lateral spacing) between film–holes
P/D	pitch–to–diameter ratio of film–hole
tke	turbulent kinetic energy (m^2/s^2)
T	local fluid static temperature (°K)
TE	trailing edge of streamwise injection film–hole at exit plane
TI	turbulence intensity (%) = $(2/3*tke)^{1/2}/V*100$
V	velocity magnitude (m/s)
y^+	non–dimensional distance away from wall
u	streamwise (x–direction) velocity component (m/s)
v	vertical (y–direction) velocity component (m/s)
w	lateral (z–direction) velocity component (m/s)
x	streamwise direction
y	vertical direction
z	lateral direction
α	injection angle (°)
Φ	compound angle (°)
η	adiabatic effectiveness = $(T_\infty-T_{aw})/(T_\infty-T_j)$
ϱ	fluid density (kg/m^3)
θ	non–dimensional temperature = $(T_\infty-T)/(T_\infty-T_j)$

Subscripts

∞	mainstream conditions at crossflow inlet plane
j	conditions at coolant supply plenum inlet plane
o	conditions in the absence of film cooling
w	conditions at wall
aw	adiabatic wall

Presented at the International Gas Turbine & Aeroengine Congress & Exhibition
Orlando, Florida — June 2–June 5, 1997

1. INTRODUCTION

Film cooling of gas turbine stator and rotor airfoil surfaces, hub and casing endwalls has played a crucial role in maintaining the structural integrity of these hot–section components at operating temperatures in excess of the melting temperature of the alloys used. The term film–cooling refers to the use of relatively cool air extracted from the latter stages of the high pressure compressor which is channeled to the turbine section and is ejected into the hot flowpath through small holes in the airfoil and endwall surfaces. Ideally, this coolant air remains close to the surface to be protected and spreads quickly between the holes to form a thin film of cool air which isolates the component from the hot combustion gases. However, the complex flow structures present at the coolant injection site often lead to lift–off or quick dilution and therefore little protection. Higher performance demands of future gas turbine designs is leading to a need for a more thorough understanding of film–cooling behavior, better databases of film–cooling performance, and truly predictive design tools. Film–cooling designs leading to increased overall effectiveness with reduced cooling air can then be implemented with more certainty.

The use of different hole geometries is one method of improving film cooling performance which has seen increased usage in the higher performance designs. Streamwise injected coolant jets through discrete holes (described in Part I) are now being turned laterally as described in the present paper (Part II), shaped (Part III), or combination of the two (Part IV) in order to extract better cooling of vital components. The purpose of this detailed four–part study is to look into these different film cooling configurations and determine the dominant physical mechanisms responsible for their performance. A row of discrete, round holes with compound angle injection is targeted in the present study for the purposes outlined above. Compound angle is implemented in modern designs to improve the spreading rate of the coolant and therefore provide more uniform coverage. However, in past studies it was found that compound angle also leads to undesirable increases in surface heat fluxes. In order to use this coolant geometry effectively, the mechanisms responsible for the contradictory surface results for adiabatic effectiveness (η) and heat transfer coefficient (h) must be fully understood so that compound angle injection can be effectively implemented in future designs with greater confidence.

Gas turbine designers are in desparate need of truly predictive design tools to test newer film–cooling concepts involving compounding, shaping, and combinations of the two for the wide range of operating conditions encountered in practice. These advanced design tools must be consistently accurate, economical, and capable of providing results with quick turnaround time. In this study, a novel implementation of computational fluid dynamics (CFD) model is validated for complex film–cooling configurations and is shown to be capable of providing reliable information regarding the relative performance of various film–cooling configurations.

2.Terminology

Due to the lack of large scale computational studies into the flowfield physics of compound–angle injection in the open literature, standard terminology designed to help readers easily adjust to the many possible orientations of the complex film cooling configurations are non existent. The present authors feel the need to define some useful terminology in an effort to improve the readability of this document.

Compound angle (Φ) is measured clockwise from the x,y–plane as shown in Figure 1. The film–hole leading edge (LE) and trailing edge (TE) points for the streamwise injection case are fixed relative to the elliptic breakout of cylindrical holes at the exit plane. As the film–hole is rotated according to the compound angle specified, the LE and TE points rotate with it as shown in Figure 1. LE and TE are used as constant reference points when discussing flow within the film–hole and at the exit plane so that the "intended" injection of the coolant is always in the direction from the leading edge to the trailing edge. "Upstream Edge" refers to the side of the film–hole upwind of the line connecting LE and TE. Similarly, the "Downstream Edge" refers to the side of the film–hole downwind of the line connecting LE and TE. Typically, the hot cross–stream fluid flows streamwise (x–direction) over the upstream edge and the coolant jet flows over the downstream edge on its way toward the test surface. The origin of the coordinate system is attached to the downstream most point on the film–hole breakout as shown in Figure 1.

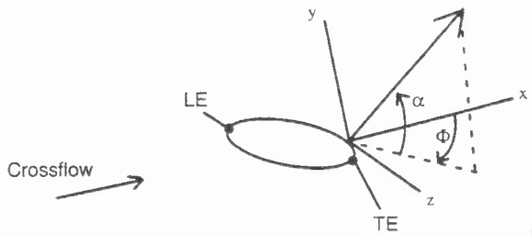

Figure 1. Demonstration of the terminology used for compound–angle injection film cooling

3. LITERATURE REVIEW

The majority of compound angle studies available in the open literature are fairly new due to the recent focus on improving film–cooling designs. As cooling technology has honed in on the need to study film–cooling configurations with realistic geometries, recent companion paper studies such as:

- Schmidt et al. (1994) study of η, Sen et al. (1994) study of h,
- Ekkad et al. (1995), two paper study of η and h, and
- Ligrani et al. (1994a) and Ligrani et al. (1994b)

have been published addressing this issue. In each of these studies surface results from select compound angle configurations were analyzed to document film cooling performance and to compare the surface results to a streamwise injection reference case. A summary of the results is included below to document the possibility that compound angle injection improves film cooling performance, and to document the need for a simultaneous examination of flowfield and surface results to explain the physical mechanisms involved.

In the study by Sen et al. (1994) and Schmidt et al. (1994), a row of film holes with α=35° and Φ=60° was compared to an equivalent streamwise injection (Φ=0°) case. Measured η results showed that the compound angle injection increased the effectiveness of the coolant. However, the heat transfer coefficient was also found to increase over the reference case. In order to combine the two results from adiabatic effectiveness and heat transfer coefficient tests to determine the ultimate effect on film–cooling performance, a heat flux reduction ratio (heat flux for a film cooled surface normalized by the heat flux for a solid surface under a simple boundary layer flow) was utilized which combined the effects of both η and h on the film–cooling performance. It was found for the case of Φ=60° that an increasing M leads to an augmentation of the heat flux entering the test surface compared to boundary layer flows, and therefore that particular film cooling configuration was completely ineffective.

Studies by Ekkad et al. (1995) provided surface results for Φ= 45° and 90° orientations. Similar to the previous studies, this work also combined the two results to provide the overall effect on the heat flux into the downstream surface. A compound angle of Φ=45° was found to actually perform better than the streamwise injection case, while the Φ=90° case was found to perform relatively poorly — despite the fact that this case provided better adiabatic effectiveness results.

Ligrani et al. (1994a, 1994b) studied a case of Φ=30° and 50.5° for both a single row and staggered double row of compound angle injected jets. Their study consisted of adiabatic effectiveness and Stanton number measurements to characterize the overall cooling performance. However, unlike the two previous works they did not combine the two types of surface results.

The only investigation which attempted to address some of the mechanisms involving film cooling with compound angle injection was a study by Lee et al. (1995) who documented the velocity field, pressure losses, and surface flow visualization for a wide range of compound angle holes. Their study was limited by the use of a single (or isolated) discrete–hole and an unrealistic length–to–diameter–ratio (L/D) of 40. In their study, velocity measurements in planes perpendicular to the crossflow path were made to document the transformation from a symmetric, counter–rotating vortices encountered in Φ=0° to a single, large vortex structure seen in Φ=90° cases. In addition, surface results were used to characterize the path of the coolant and its interaction with the crossflow.

4. OUTSTANDING ISSUES

It can be concluded from the above studies that compound angle injection can provide better film–cooling performance such as the case shown for Φ=45° by Han et al. (1995). In some cases, however, compound angle injection leads to such high heat transfer coefficients that it would be better to introduce no film cooling at all as in the case of Φ=60° and M=2.0 documented by Sen et al. (1994). Clearly, there are a number of studies with contradictory observations regarding the effects of compound angles in film cooling. Although the above studies provide a database of information describing the surface results, they do not document the physical mechanisms responsible for the outcome. Only a simultaneous, in–depth examination of the flowfield and surface results can provide this type of analysis to gas turbine designers. Such understanding is crucial to extending the results of the simplified flat plate studies to the more complex operating environment of gas turbines. Finally modern computational fluid dynamics methodologies developed to enable the gas turbine designers to accurately assess the relative performance of different compound angle configurations has not at all been resolved in the open literature.

5. PRESENT CONTRIBUTIONS

The primary goals of this four part study are to: (i) uncover the dominant flowfield mechanisms responsible for the surface adiabatic effectiveness and heat transfer coefficient distributions; (ii) demonstrate the capability of computational fluid dynamics in providing consistently accurate results to distinguish between various film cooling configurations. The specific contributions of the present study are as follows:

- validation of a state–of–the–art computational methodology to predict η and h for compound–angle injection film cooling;
- documentation of the dominant physical mechanisms influencing the film cooling behavior with a novel use of the vorticity concept;
- description of the effects of varying the Φ angle on the dominant mechanisms and on the surface results;
- determination of the effects of blowing ratio (M) on film cooling behavior for various Φ angles;
- comparisons of the relative performance of different film cooling configurations; and
- establishment of a predictive computational design methodology.

To accomplish the stated objectives, results for compound–angle injection cases of Φ=45°, 60°, and 90° are computationally compared to a streamwise reference case (Φ=0°) and also to experimentally measured data obtained in–house and in the open literature. These geometries are demonstrated in Figure 2 by a single pitch of the the row of holes studied.

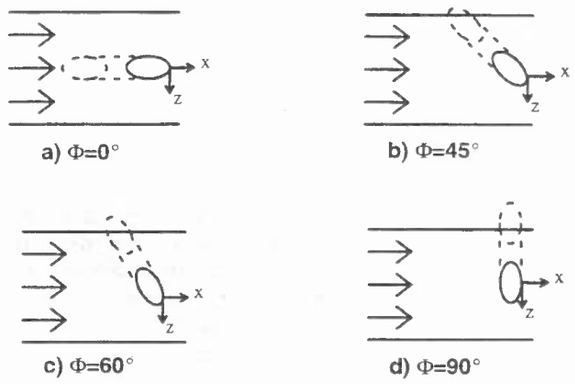

Figure 2. Top view of a single pitch of a row of holes showing the four film cooling configurations studied.

6. SIMULATION DETAILS

The computational methodology implemented in the present research was developed and validated for studying jet–crossflow interactions as described by Butkiewicz et al. (1995), Walters et al. (1995), Hyams et al. (1996), and Walters and Leylek (1996). Consistent with those studies, the NURBS based solid modeling software, I–DEAS, by SDRC Inc. was utilized to accurately capture the geometry including the film–hole, plenum, and crossflow regions. I–DEAS was then used to generate a high quality and high density background grid mesh in this complex and rather large computation domain. The actual CFD analysis was performed using Fluent/UNS solver by Fluent Inc. which is a pressure–correction based, multi–block, multigrid, unstructured/adaptive solver. The higher order linear reconstructive discretization scheme was used to reduce numerical viscosity and to better capture all gradients. Turbulence closure was attained using standard(or high Reynolds number) k–ε turbulence model in conjunction with the generalized wall–functions. Strict convergence criterion were met in which:

- global mass and energy imbalances were brought below 0.01%;
- residuals normalized by inlet fluxes were brought below 0.1%; and
- dependent variables monitored in important areas of the flowfield were shown to not change with further iterations.

Also grid independence was established within Fluent/UNS by adapting to the highest gradient regions of the flow field and monitoring the variables to ensure that the dependent variables changed less than 5% at monitored locations. A hanging–node adaption procedure was used which maintained the high quality of the initial background grid. Typically, a background grid consisted of approximately 300,000 cells with the majority of the cells in the jet–crossflow interaction region. The final grid,

which provided a "grid–independent" solution, contained approximately 620,000 cells with the majority of adaptions in the film–hole and the near–field regions. For more details of the computational methodology the reader is encouraged to study the reference papers published by the Clemson group cited above. The unique aspects of the present work are included below to extend the established methodology to the study of compound angle injection.

Computational Model

The computational models were constructed as the exact replicas of the experimental counterparts for all cases. Nondimensional parameters such as the lateral spacing between holes, P/D=3, and the length of the film hole, L/D=4.0, were consistent amongst all the models. Due to the symmetric nature of film cooling with a row of holes with streamwise injection (Φ=0°), the computational domain was reduced to a half–pitch simulation between two symmetry planes. For the compound angle cases (Φ>0°), a full–pitch was modeled and repeating boundary conditions were applied between holes as shown in Figure 3. A zero normal gradient condition was imposed at 10D above the test surface where it was determined to be far enough away to not affect the jet–crossflow interaction. The test section downstream of the film–hole TE was extended to 25D where a convective outflow (upwinding) condition was applied which allowed the jet–crossflow interaction to be documented far downstream of the coolant exit plane. The film–hole diameter, flow conditions, and plenum geometry differed slightly between the experimental cases modeled and are described separately for each study documented below.

Φ=0° and 60°. For the computational study of Φ=0° and 60° cases, the geometry and operating parameters exactly matched to the experimental works of Schmidt et al. (1994). Using a hole diameter of 11.1 mm, a one–dimensional flow concept was used to set the plenum inlet velocity to achieve an average velocity of 11.75 m/s within the metering section of the film hole. The plenum dimensions in the x–, z–, and y–directions were 9.15D wide by 3D deep by 4.57D high, respectively. In order to match the upstream boundary layer development of the University of Texas experiments a turbulent boundary layer was started at 23.1D upstream of the streamwise hole by applying a uniform velocity inlet condition there. Crossflow velocities were set to obtain the desired blowing ratio based on the film–hole nominal velocity 11.75 m/s and Re=18,717.

Φ=45° and 90°. For the compound angle configurations Φ=45° and 90°, the geometry and operating parameters were modeled to correspond with experiments from Clemson University, Farmer et al. (1997). The crossflow was introduced at 300 K and with a freestream velocity of 25 m/s. In order to match the boundary layer thickness of 0.7D at the film–hole LE, a $1/7^{th}$ law turbulent boundary layer velocity profile was applied at 10D upstream of the leading edge of the film–hole based on actual data obtained at that location. Plenum inlet velocity was then varied to give the desired film–hole nominal velocity to set the blowing ratio using a hole diameter of 8.3 mm.

Grid Generation.

The solid model of every film cooling geometry was divided into a large number of subregions within I–DEAS in order to obtain a high quality grid as discussed in Walters and Leylek (1996). In this study, some additional steps were taken within I–DEAS in order to apply the periodic boundary conditions properly in Fluent/UNS. Regions had to be added with the stipulation that corresponding surfaces on the periodic walls matched perfectly across the film cooling passage. The "Surface Dependency" feature in I–DEAS was applied to these periodic walls to ensure that nodes and cells on these surfaces were built with the same nodal and cell distribution. (The reader is encouraged to reference the I–DEAS users manual for more information on this feature.)

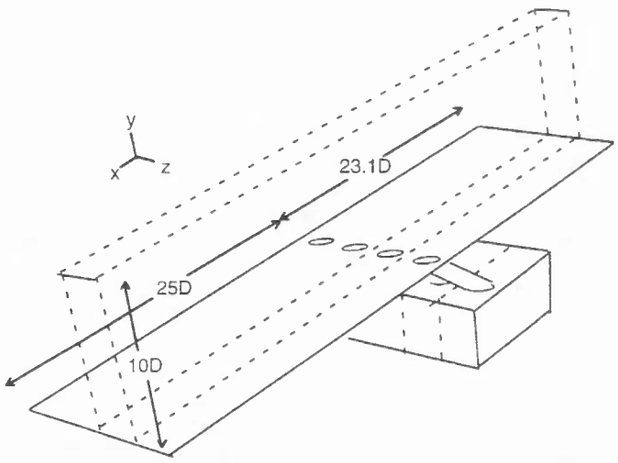

Figure 3. Isometric view of the computational domain aft looking forward showing the extentof the domain for Φ=60°.

7. EXPERIMENTS USED FOR VALIDATION

The computational simulations were validated by comparisons to both in–house experimental work at Clemson University and companion studies by Schmidt et al. (1994) and Sen et al. (1994) from The University of Texas at Austin. These two sources of experimental data employed two completely different measurement techniques for determining the surface results as discussed below.

7.1 In–House Experimental Work

Experiments were carried out at Clemson University to measure both the adiabatic effectiveness in a 0.6m x 0.6m low speed wind tunnel. The experimental setup implemented used a hue based thermochromic liquid crystal temperature measurement method. A low conductivity substrate material test plate was coated with a layer of liquid crystals with a temperature bandwidth between 15° C and 20° C. A real time image capturing system was used to calibrate the liquid crystal's temperature response to the corresponding hue values. A density ratio (DR) of 1.55 was obtained through the injection of CO_2 gas into an ambient air mainstream flow. The foreign gas was injected at various temperatures below the liquid crystal bandwidth to achieve the desired hue response. M=1.25 and M=1.88 were obtained by varying the flow rate of the foreign gas, while the mainstream velocity was held constant at 10 m/s. The adiabatic effectiveness was calculated based on T_∞, T_j, and T_{aw} under steady state operating conditions.

7.2 Experimental Setup for Schmidt et al. (1994)

The research efforts at the University of Texas modeled film cooling behavior using cryogenically cooled air (T=187.5 K) injected into ambient air crossflow resulting in a DR=1.6. Adiabatic effectiveness results

were calculated from temperature measurements made by thermocouples imbedded in the downstream wall. For the determination of h, ambient air was used as the injectant at a DR=1.0. The momentum flux ratio, J=0.98 was used as a scaling parameter to combine the η results at DR=1.6 and M=1.25 and the h results at DR=1.0 and M=1.0 to calculate a Net Heat Flux Reduction (NHFR) parameter, $NHFR=1-h/h_0(1-\eta\theta_\infty)$.

8. RESULTS AND DISCUSSION

Flow in the Film–hole

The flow field developed at the entrance to the film hole was shown in Walters et al. (1995) to be complex and very dependent on the operating conditions. The complexities in this region are primarily due to the flowpath design. Coolant is channeled to the film hole through a plenum which is much larger in volume than the film hole itself, and therefore, as the coolant enters into the film hole it is strongly accelerated. Along with this velocity increase there is excessive turning at the sharp–edged entrance to the film–hole. At an injection angle of 35°, some of the coolant has to go through a turn of 145° into the film hole at the downstream side of the plenum. The inability of the coolant to negotiate this turn leads to a large 3–D separation along the downstream surface of the film–hole. This separation region results in:

- nonuniform coolant distribution
- secondary motion within the film–hole
- high velocity gradients
- high turbulence generation.

The mechanisms discussed above are primarily dominated by the flow at the entrance to the film–hole. As the film–hole is rotated to provide lateral momentum to the coolant fluid in the compound–angle injection cases, the entrance region remains essentially unchanged except the location of the separation region relative to the plenum. The flow at the entrance and throughout the majority of the film–hole are unaffected by the large changes in the exit conditions brought about by the compound angle injection. One method of demonstrating this is to examine the parameters along the film–hole centerline planes. The definition of the film–hole centerline plane is shown in Figure 4 for Φ=60°. In Figure 5 the velocity contours along the film–hole centerline plane show the similarity of the flow between the two configurations for both the Φ=0° and Φ=60° case. Similarly, good correspondence was also found for the turbulence intensity and the secondary flow structures described for the streamwise injection case in Walters et al. (1996).

Exit Conditions

As the coolant approaches the exit plane of the film–hole, the coolant flow deviates considerably from the streamwise injection case due to significant changes in the pressure field at the exit. The physical explanation for the pressure changes shown in Figure 6 is given in the near–field evaluation. As the compound angle is increased the pressure field imposed at the jet exit is changed in the following three ways:

- the upstream high pressure region acts across a wider area of the film–hole breakout,
- the downstream low pressure decreases even further behind the film–hole breakout, and
- the streamwise pressure gradients increase due to a decrease in the streamwise breakout distance between the pressure extremes, as Φ is increased.

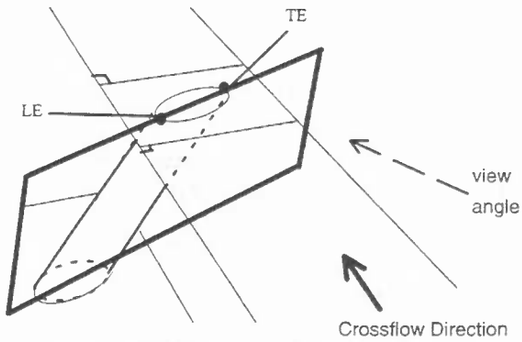

Figure 4. Demonstration of the film–hole centerline plane for Φ=60°.

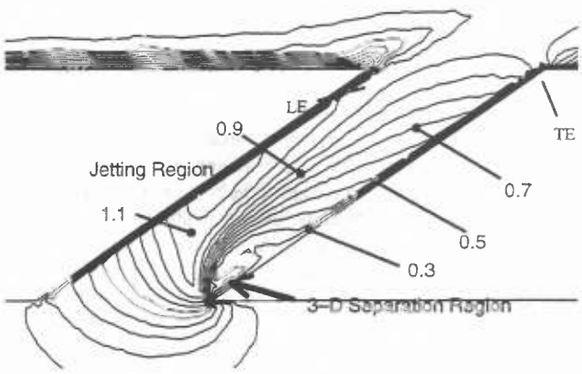

a) Φ=0°, M=1.25

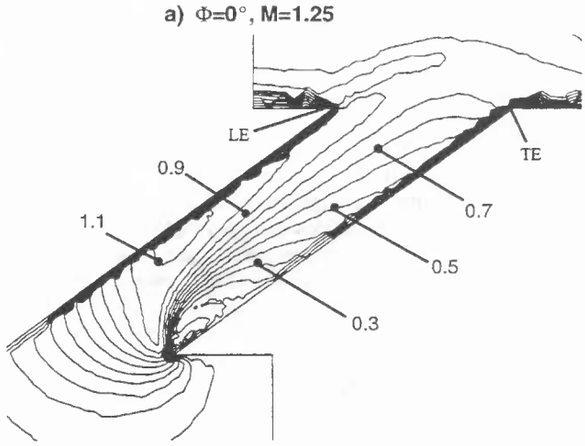

b) Φ=60°, M=1.25

Figure 5. Velocity magnitude normalized by U_∞ showingjetting and separation regions demonstrating very goodcorrespondence between a) the streamwise Φ=0° andb) the Φ=60° compound–angle cases.

These changes in the pressure field cause higher blockage at the exit which leads to deviations of the coolant trajectory after it leaves the film–hole. The case of Φ=45° and Φ=60°resemble the Cp contours depicted for Φ=90°.

Coolant Distribution. The coolant distribution at the exit is determined by two competing mechanisms:

- the nonuniform distribution of coolant within the film hole due to the separation region at the inlet to the film hole, and
- exit plane blockage due to pressure gradients caused by the crossflow impinging on the coolant.

As can be seen in the streamwise case in Figure 5a the separation region at the inlet to the film–hole leads to a jetting effect along the upstream edge of the wall. Due to the short L/D=4.0 the relatively high momentum jetting fluid does not completely diffuse out across the film hole and therefore is still evident even at the coolant exit plane. In Figure 7 the effective coolant distribution at the exit is shown by contours of normalized v, or vertical velocity component. Little variation of v at the exit is seen due to the balance of the effects of high momentum jetting fluid mentioned near the leading edge and streamwise pressure gradients due to crossflow impingement. This distribution is dependent on operating conditions as discussed in Walters et al. (1996).

For the same operating conditions, compound–angle film cooling can be seen to be more strongly affected by the pressure gradients and blockage at the exit plane. The blockage is stronger because it acts over a larger area and therefore the coolant is forced to exit near the downstream edge of the film hole. The smaller effective exit area leads to an increase in v near the downstream edge of the hole and little coolant exiting from the upstream edge. Because of the orientation of the hole, the jetting fluid is now forced to exit along the downstream edge of the film hole near the LE point and there is no opportunity to have the balance of blockage and jetting seen in the streamwise case.

Coolant Trajectory

Compound Discharge Angle (Φ). The jet trajectory is so strongly affected by the pressure distribution that very little of the fluid exited with the intended film–hole metal angle for all the cases studied. The deviation of the coolant trajectory from the compound–angle of the metal is shown in Figure 8 for the case of Φ=90°. The coolant compound angle trajectory at the exit ranges from 40° (approximately half of the metal angle) near the TE, to almost the metal angle of 85° at the upstream side of the LE. This trend was consistent in both computational and experimental results for all of the compound angle cases studied. The coolant near the trailing edge region exited at a very shallow compound angle due to its low momentum which allowed it to be turned by the crossflow accelerating between the holes. This will prove to be important in explaining the results for adiabatic effectiveness and heat transfer coefficient in later sections. The area of highest compound discharge angle at the exit plane coincides with the upstream edge near the LE point. Coolant is not able to negotiate the high pressure gradients seen and therefore flows almost parallel to the film hole exit plane towards the trailing edge.

Streamwise Discharge Angle (α). The streamwise discharge angle of the coolant at the film–hole exit–plane showed a similar dependence on the presence of high pressure blockage and jetting fluid regions. The low injection angles, α<35° are all seen along the upstream edge of the film–hole where blockage due to the high pressure regions leads to low vertical momentum. However, near the downstream edge the coolant exits at α>35° where jetting fluid is being forced to exit due to the reduction in the effective exit area of the film hole by blockage.

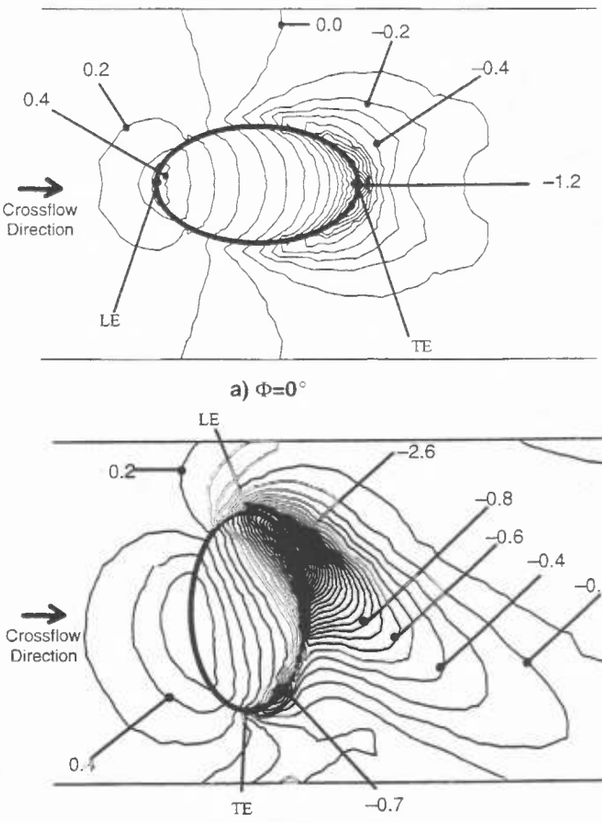

Figure 6. Cp along the test surface showing increased pressure gradients between a)Φ=0° and b) Φ=90° at M=1.25 .

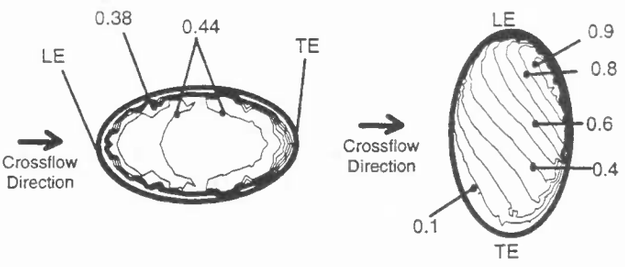

Figure 7. v/U_∞ for the case of M=1.25 showing the effects of compound–angle injection on the coolant distribution at the exit for a) Φ=0°, and b) Φ=90°.

Near–field Behavior

The near–field behavior of jet–crossflow interactions with compound angle injection is dominated by:

- the vorticity contained within the film–hole boundary layers;
- the vorticity generated at the interface of the coolant and the crossflow along the downstream edge near the LE point;

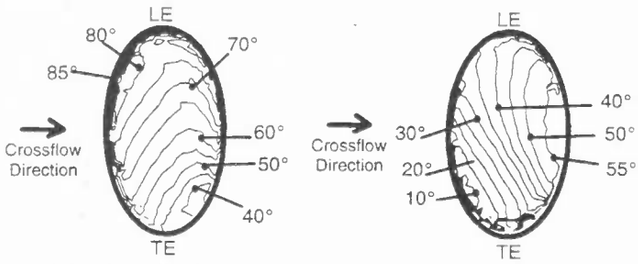

Figure 8. Discharge angles showing the jet trajectory as it exits the film hole for the case of Φ=90°, M=1.25.

- the pressure field set up in the jet–crossflow interaction; and
- the turbulence generated in the shear layers between the jet and crossflow.

The vorticity sources are responsible for the strength of the secondary flow structures which degrade the coolant and cause rapid spreading downstream of the film–hole. The pressure field dominates the general path taken by the crossflow and coolant as the two interact. The turbulence generated leads to a decrease in η by enhancing diffusion of the coolant toward the wall and an increase in h due to elevated turbulence near the wall. These three mechanisms will be described separately below as they relate to the nearfield behavior shown in Figure 9 by of particles traces released from the boundary layer of the oncoming crossflow flowing over an isothermal surface Θ=0.2 which caracterizes the coolant path.

Effects of Vorticity. The vorticity field in compound angle injection is significantly different from the streamwise injection cases with cylindrical and shaped holes documented in the companion papers designated as Part I and Part III. For the streamwise injection cases, it was shown that the primary cause of the symmetric counter–rotating vortex structures seen downstream of the jet/crossflow interaction site was the vorticity emanating from the film–hole boundary layers. In compound–angle injection, a new mechanism for streamwise vorticity appears at the interface region between the crossflow and coolant jet on the downstream side of LE. The strength of this new source increases with increasing Φ. The relative strength of the two vorticity sources is configuration dependent. With compound–angle injection, the originally symmetric counter–rotating vortex structure becomes increasingly asymmetric as Φ increases and eventually turns into a single vortex at Φ=90°. It is the positive x–direction vorticity along the upstream edge that is inhibited by compound–angle injection. Therefore, the counter–clockwise rotating leg (looking upstream) of the secondary flow structure starts shrinking with increasing Φ and collapses completely at Φ=90°.

In compound–angle injection, the strong side of the vortex lies along the downstream edge and the weak vortex along the upstream edge of the film–hole. The increase in the strength of the downstream edge vortex is caused by the fact that as the film hole is turned laterally at increasing Φ, the crossflow fluid flows perpendicular to the coolant flow direction as it negotiates over and around the leading edge side as shown in Figure 9. Because of the good alignment of the vorticity generated at this interface and the local velocity field, this particular interaction plays a more dominant role. In addition, the crossflow fluid flows parallel to the downstream edge all the way around the film–hole resulting in a coalescing of the vorticity. This vorticity generates a single large rotating vortex structure in the near field whose center lies slightly behind the exiting jet. As the coolant is turned toward the downstream and bent over, the vorticity aligns itself with the coolant path which, as described earlier, is along a direction at half the compound angle of the metal (for the case of M=1.25, DR=1.6).

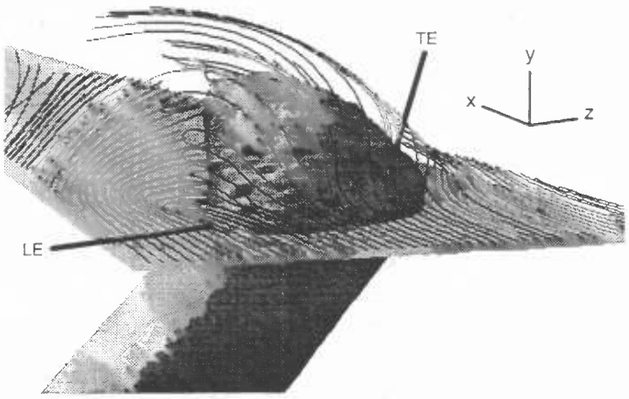

Figure 9. Particle traces released from the crossflow boundary layer showing the complex flow around an isotherm Θ=0.2 for M=1.25 and Φ=60°.

The weakening of the upstream edge vortex was attributed to its dependence on the vorticity emanating from the film–hole boundary layer along this surface. As the film hole is turned laterally, the effective coallescing of vorticity is reduced due to the fact that:

- the long surface of the film hole is turned toward the crossflow causing the boundary layer vorticity to get blocked by the stagnation region formed at the upstream edge; and
- the coolant trajectory is very shallow along the upstream edge of the film hole resulting in a shift in the vorticity vector direction.

As the compound–angle is increased to 60° and 90° the weak vortex disappears due to these mechanisms.

Effects of Pressure. As the oncoming crossflow impinges on the exiting coolant, it is forced either between the film–holes or over the jets due to the large pressure rise set–up along the upstream edges of the jets as shown in Figure 6. As the compound angle is increased, the high pressure region becomes wider and more of the crossflow is forced over the jets. Also the remaining crossflow fluid which flows between holes is forced through an effective spacing which decreases with increasing Φ and is subjected to sharper turning angles. This high pressure region also continues to affect the coolant fluid after it exits the film–hole by quickly forcing the coolant to begin bending down toward the test surface and also toward the downstream direction. The bending of the jet as it exits the film–hole leads to two low pressure regions behind the film–hole. The first of these is on the downstream side of the LE point where the jetting fluid exits at the highest injection angle and lifts off immediately. The separating coolant jet is quickly bent over resulting in a low pressure region under its curved streamlines. This low pressure pocket sucks the upstream crossflow fluid right under the jet inducing lateral momentum which will be shown to be present even in the far–field. The second low pressure region is near the downstream side of the TE point where the low momentum coolant exits and is being turned toward the streamwise direction by the crossflow fluid accelerating between two adjacent film–holes.

Turbulence Generation. The two major sources of turbulence are the film–hole generated turbulence and the turbulence generated in the high velocity gradient region on the downstream edge near LE as shown in Figure 10. In the near–field, the high turbulence present close to the test surface is dominated by the latter due to the following two reasons:

- the turbulence in this region does not have a chance to attenuate due to its close proximity to the high velocity gradients fueling turbulence at the jet–crossflow interface; and
- the flow from the high turbulence region remains close to the wall due to the coolant being bent over the top of it.

Because this high turbulence lies underneath the coolant it will aid in diffusing the coolant toward the wall to improve η. However, it will also tend to increase h in these regions as will be discussed in the surface results. Turbulence generated within the film–hole is convected out and deposited in the center of the coolant core. Since there are no shear layers to sustain it, this particular turbulence pocket quickly diffuses and dissipates throughout the core region. It only plays a small role in the surface results when it is carried toward the surface by the vortex structure.

Far–field Behavior

The far–field behavior is dominated by the flow structures set up in the near field. In the streamwise case discussed in the companion paper (Part I), the far–field behavior is shown to be strongly dominated by a counter–rotating vortex structure which tends to lift the coolant off the surface to be protected. In compound angle cases, this counter–rotating vortex becomes asymmetric and actually collapses to a single rotating vortex with significant lateral motion of coolant near the wall. The single vortex structure continues to play a role in the far field by convectively mixing the coolant and the crossflow leading to a relatively uniform lateral distribution of temperature as shown in Figure 11. The vortex loses its strength with downstream distance and eventually the flow becomes a crossplane shear layer between the streamwise freestream and the lateral motion near the test surface, Figure 12.

Surface Results

Adiabatic Effectiveness. The surface results examined in this paper consist of η and h distributions along the downstream test surface. The coolant distribution on the test surface shown in Figure 13 can be characterized by three primary regions:

1. The first region is the low momentum coolant fluid which oozed out of the trailing edge of the film hole and remained attached. This coolant is deteriorated with downstream distance by secondary flow;
2. The second region is a hot region as a result of hot crossflow fluid tucking under the coolant along the downstream edge of the film hole starting at LE; and
3. The third region is caused by the coolant core lifting off and returning to the wall downstream through diffusion and secondary flow convection.

In region 1, the trajectory setup in the near–field is roughly seen to hold with the surface results downstream. The coolant follows a path approximately half of the compound–angle of the metal. These trends are shown in Figure 14 for both the experimental and computational data with only slight deviations in magnitude and lateral motion. The computations consistently predicted lower η results between film–holes in the near–

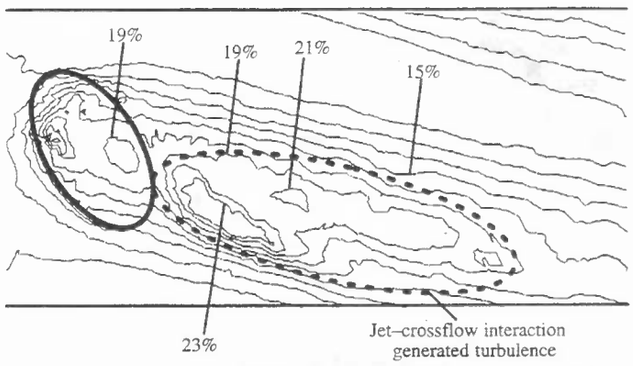

Figure 10. Turbulence intensity on a plane y/D=.2 showing turbulence quantities exiting the film–hole as well as those generated by the jet–crossflow interaction for M=1.25, Φ=60°.

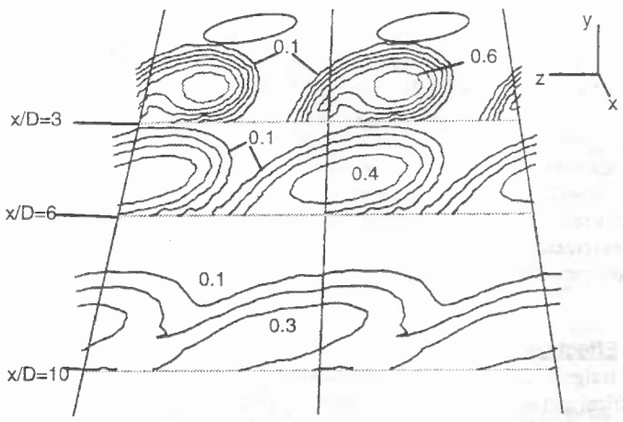

Figure 11. Contours of θ at downstream locations showing a quick merger of coolant between holes for Φ=60°, M=1.25.

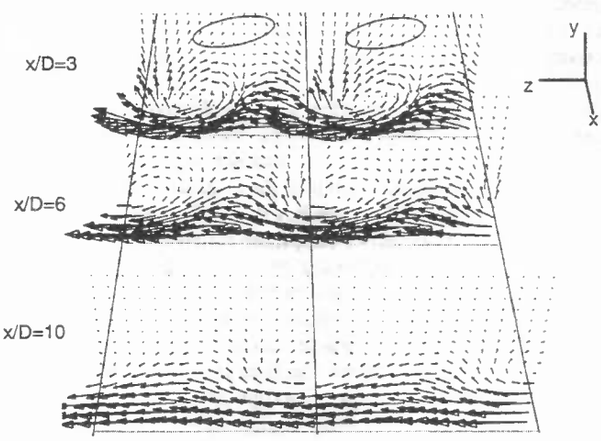

Figure 12. Velocity vectors in crossplanes showing the demise of the vortex as it is damped to a pure lateral shear layer for M=1.25, Φ=60°.

field region and a higher, narrower attached region. These deviations are attributed partly to insufficient spreading in the computations and also the limited ability of creating perfectly adiabatic surfaces in experiments. It can also be seen in Figure 14 that the lateral motion is underpredicted. The η results for the other cases studied are shown in the laterally averaged $\overline{\eta}$ in Figure 15. Increasing the compound angle leads to a narrower attached region and therefore lower values of $\overline{\eta}$ in the near field. The compound angle had positive effects with downstream distance by causing the coolant core to be convected and diffused toward the surface more quickly leading to an increase in $\overline{\eta}$. Blowing ratio tended to cause region 1 to decrease quicker due to increased jetting effects leading to a decrease in $\overline{\eta}$ the nearfield, however the increase in coolant does lead to higher $\overline{\eta}$ farther downstream as the core returns to the protected surface.

Heat Transfer Coefficient. Compound–angle injection was found to significantly alter the heat transfer coefficient results. For example, due to the presence of an unique turbulence generation mechanisms, turbulence at the wall is significantly increased where the crossflow accelerates underneath the coolant. This factor leads to increased h/h_o values in Figure 16 in regions where the highest temperatures are found in Figure 13. Validation of these results was provided by comparisons of a DR=1.0, M=1.0 case to the equivalent case by Sen et al. (1994) in Figure 17 showing good correspondence. Also the laterally averaged value of h/h_o was utilized to compare the different configurations studied in Figure 18.

9. CONCLUSIONS

Large scale computational simulations with high density and high quality grid meshes were carried out for film cooling configurations with a row of cylindrical holes involving compound–angle injections at Φ=45°, 60°, and 90°. Predicted results were validated against experimental data and compared to the reference case of streamwise injected coolant jets. The key set of conclusions drawn in this study are as follows:

- η and h distribution on the test surface is dominated by the vortex structure found downstream of the jet–crossflow interaction site;
- as Φ increases the well–known symmetric counter–rotating vortex structure becomes increasingly asymmetric as one leg collapses and the other one forms a single dominant vortex at Φ=90°;
- the collapsing leg is associated with vorticity along the upstream edge of the film–hole which is blocked due to a large stagnation region created by the crossflow impinging on the coolant jet;
- an important second source of vorticity is found at the interface of crossflow and coolant jet along the downstream edge near the LE point. This vorticity augments the one in the film–hole boundary layer and strengthens as the compound–angle increases. Relative magnitudes of the two vorticity sources is configuration dependent;
- compounding improves the lateral uniformity of the adiabatic effectiveness. At high Φ angles, the lateral distribution of η is ruler–flat within only a few diameters downstream of the row of film–holes; and
- the heat transfer coefficient was found to be augmented due to the compounding effects in all the cases studied; however, there is net gain as the compound–angle injection is capable of providing a highly sought–after feature in film cooling, namely, lateral spreading and uniformity.

ACKNOWLEDGMENTS

This paper was prepared with the support of the U.S. Department of Energy, Morgantown Energy Technology Center, Cooperative Agreement No. DE–FC21–92MC29061. The authors would like to thank Clemson University graduate students Mr. John Farmer and Mr. Dave Seager, as well as their faculty advisor Prof. James A. Liburdy for the experimental data used in the present study. Also, special thanks are due to Mr. Gary Berger and Mr. Richard Baldwin of CNS at Clemson University and John Lane of the University of South Carolina for their assistance in computer related matters. We are also deeply indebted to Dr. Rick Lounsbury at Fluent, Inc. for his invaluable support with Fluent/UNS.

REFERENCES

Butkiewicz, J., Walters, D., McGovern, K., and Leylek, J., 1995, "A Systematic Computational Methodology Applied to a Jet–in–Crossflow Part 1: Structured Grid Approach," Presented at the ASME Winter Annual Meeting, San Francisco, CA., November 17, 1995

Ekkad, S., Zapata, D., and Han, J., 1995, "Film Effectiveness Over a Flat Surface with Air and CO2 Injection through Compound Angle Holes Using a Transient Liquid Crystal Image Method," ASME Paper No. 95–GT–11.

Ekkad, S., Zapata, D., and Han, J., 1995, "Heat Transfer Coefficients Over a Flat Surface with Air and CO2 Injection through Compound Angle Holes Using a Transient Liquid Crystal Image Method," ASME Paper No. 95–GT–10.

Hyams, D., McGovern, K., and Leylek, J., "Effects of Geometry on Slot–Jet Film Cooling Performance," ASME Paper No. 96–GT–187.

Lee, S., Kim, Y., Lee, J., 1995, "Flow Characteristics and Aerodynamic Losses of Film–Cooling Jets with Compound Angle Orientations," ASME Paper No. 95–GT–38.

Ligrani, P., Wigle, J., Ciriello, S., and Jackson, S., 1994, "Film Cooling from Holes with Compound Angle Orientations, Part I: Results Downstream of Two Staggered Rows of Holes with 3D Spanwise Spacing," ASME Journal of Heat Transfer, Vol. 116, pp. 341–352.

Ligrani, P., Wigle, J., and Jackson, S., 1994a, "Film Cooling from Holes with Compound Angle Orientations, Part II: Results Downstream of a Single Row of Holes with 6D Spanwise Spacing," ASME Journal of Heat Transfer, Vol. 116, pp. 353–362.

Fluent–UNS Users Guide, May 1996, Release 4.0, Fluent Incorporated, Lebanon, NH.

Schmidt, D., Sen, B., and Bogard, D., 1994, "Film Cooling with Compound Angle Holes: Adiabatic Effectiveness," ASME Paper No. 94–GT–312.

Sen, B., Schmidt, D., and Bogard, D., 1994, "Film Cooling with Compound Angle Holes: Heat Transfer," ASME Paper No. 94–GT–311.

Walters, D., and Leylek, J., 1996, "A Consistently Accurate Computational Methodology Applied to a Three Dimensional Film Cooling Flowfield," ASME Paper No. 96–GT–351.

Walters, D., McGovern, K., Butkiewicz, J., and Leylek, J., 1995, "A Systematic Computational Methodology Applied to a Jet–in–Crossflow Part 2: Unstructured/Adaptive Grid Approach," Presented at the ASME Winter Annual Meeting, San Francisco, CA.

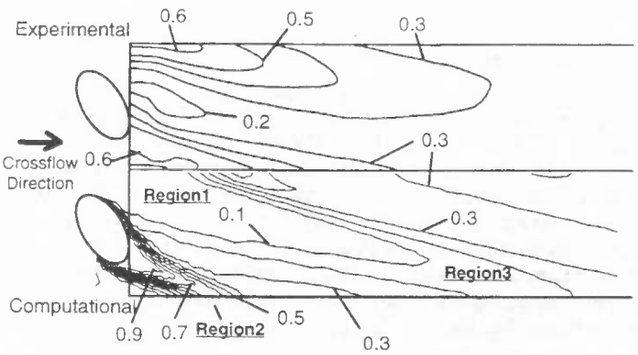

Figure 13. Contours of η on the downstream wall showing the characteristic regions for both computations (bottom) and experiments (top) for Φ=60° and M=1.25.

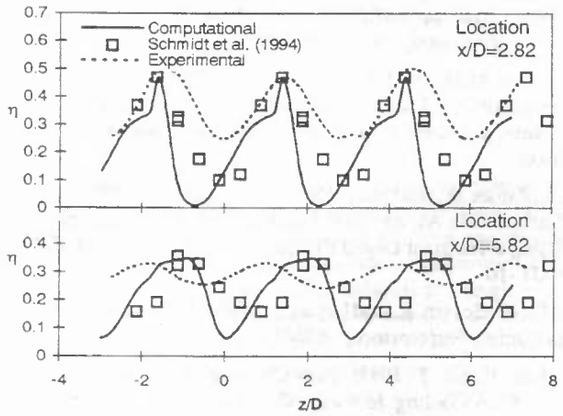

Figure 14. Lateral distribution of η at downstream locations showing good correspondence between experiments and computations for Φ=60° and M=1.25.

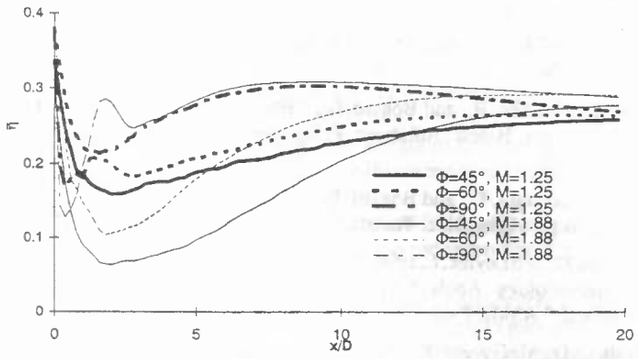

Figure 15. Laterally averaged $\bar{\eta}$ versus downstream distance showing the effects of compound-angle injection Φ and blowing ratio.

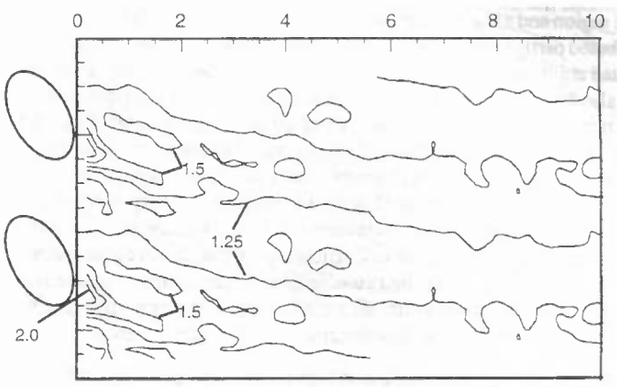

Figure 16. Normalized heat transfer coefficient for M=1.25, and Φ=60°

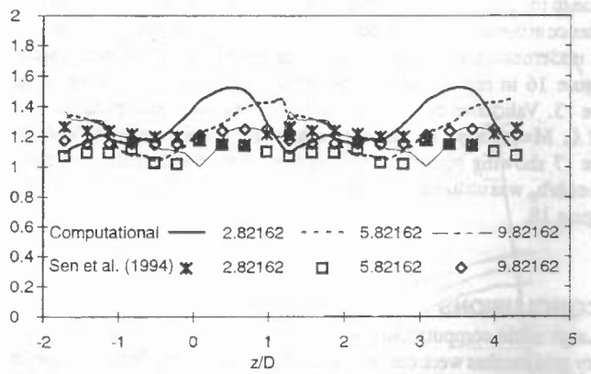

Figure 17. Lateral distribution of heat transfer coefficient show good agreement between computationally predicted and experimentally measured data.

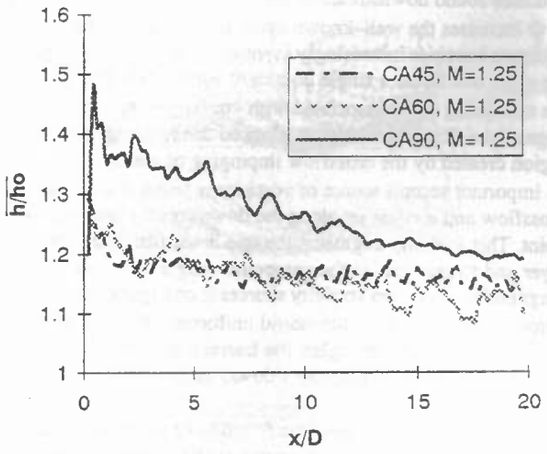

Figure 18. Laterally averaged heat transfer coefficient results showing the effects of compound angle on the heat transfer caracteristics.